



Restricted piperazine diffusion by polyacrylic acid for high flux nanofiltration membrane

Ziliang Fan, Fangwei Chen, Wentao Yan, Yong Zhou*, Congjie Gao

Center for Membrane and Water Science and Technology, Zhejiang University of Technology, Hangzhou 310014, China, Tel.: +86-13858061565; emails: zhouy@zjut.edu.cn (Y. Zhou), 2112001384@zjut.edu.cn (Z.L. Fan), chenfw@zjut.edu.cn (F.W. Chen), yanwentao@zjut.edu.cn (W.T. Yan), gaocj@zjut.edu.cn (C.J. Gao)

Received 1 November 2022; Accepted 5 March 2023

ABSTRACT

Increasing the water flux of nanofiltration membrane is of great significance for expanding the application field of nanofiltration membrane, reducing energy consumption and building a conservation-oriented society. Polyamide nanofiltration membrane prepared by traditional interfacial polymerization has many problems, such as dense internal structure and poor water permeability. In this study, polyacrylic acid (PAA) was introduced into the interfacial polymerization. There are electrostatic and hydrogen bond interactions between PAA and piperazine (PIP). At the same time, the polymer properties of PAA increase the viscosity of aqueous solution. Under the joint action of two factors, the diffusion of PIP to the organic phase was effectively restricted. A thin (~62 nm) separation layer was prepared to improve the water flux of the nanofiltration membrane. In addition, the introduction of PAA also enhanced the hydrophilicity and electronegativity of the membrane surface. The results showed that the optimum addition of PAA was 0.15 wt.%, and under the working condition of 25°C and 0.5 MPa, the pure water flux of the PAA_0.15@PA membrane is 80.18 L·m⁻²·h⁻¹, which is nearly 25% higher than that of pristine PA membrane. The salt rejection order is Na₂SO₄ > MgSO₄ > NaCl > MgCl₂, which is a typical negatively charged nanofiltration membrane. The PAA_0.15@PA membrane has a narrow pore-size distribution, has a high rejection rate for small molecule (180–400 Da) organics while maintaining a high flux, and has good separation stability.

Keywords: Nanofiltration; Polyacrylic acid; Piperazine diffusion; Interfacial polymerization; High flux

1. Introduction

As a new type of separation membrane, nanofiltration membrane has a pore diameter of 0.5–2 nm, and has good rejection performance for substances with molecular weight of 200–2,000 Da [1,2]. The operating pressure is generally 0.1–1 MPa, which is widely used in seawater desalination, dye separation, wastewater treatment and other fields [3–5].

Interfacial polymerization (IP) is a common method for industrial production of nanofiltration membrane.

Polyamide composite membrane prepared by interfacial polymerization is a typical representative of nanofiltration membrane materials at present, which is generally composed of porous support layer and separation layer [6–9]. The principle of this method was proposed by Morgan [10] in 1965, and Cadotte [11] used this method to prepare the first composite membrane in 1970. However, the polyamide nanofiltration membrane prepared by traditional interfacial polymerization has many problems, such as dense internal structure, high mass transfer resistance and poor water permeability [12–14]. The permeability of nanofiltration

* Corresponding author.

membrane is closely related to the energy consumption of the filtration system. Improving the water flux of nanofiltration membrane is of great significance for reducing the energy consumption of the system, saving the operation cost and expanding the application range [15–17].

In a conventional IP process, the amine monomer in the aqueous phase rapidly diffuses to the two-phase interface within a certain time and reacts with the acyl chloride monomer in the organic phase to form a polyamide (PA) layer. The nanofiltration membrane thus prepared often shows a low permeability flux. Therefore, effective control of amine monomer diffusion and interface reaction rate is the key to optimize PA layer and improve the separation performance of nanofiltration membrane. In recent years, researchers often restrict the diffusion of piperazine (PIP) monomer by introducing aqueous additives. For example, Zhang et al. [18] used polyvinyl alcohol (PVA) as a hydrophilic macromolecule to inhibit the diffusion of reactants, and prepared a nanofiltration membrane with a desalination and water purification performance more than three times higher than the traditional nanofiltration membrane and a nano Turing structure. Li et al. [19] prepared thin-film composite (TFC) membrane by interfacial polymerization on HKUST-1 MOF interlayer. The MOF interlayer restricted the diffusion of PIP and formed a thin and highly cross-linked polyamide separation layer. Zhu et al. [20] added porous organic polymers (o-POPs) and PIP into casting fluid to prepare polymer substrate, and prepared o-POPs modified thin-film nanocomposite (TFN) membrane by interfacial polymerization. Under the optimal conditions, the water permeability of TFN membrane is $29.6 \text{ L}\cdot\text{m}^{-2}\cdot\text{h}^{-1}\cdot\text{bar}^{-1}$. Van et al. [21] took the hydrogel containing piperazine monomer as the aqueous phase, and the hydrogel in the interfacial polymerization reduced the diffusion rate of PIP, and prepared the ultra-high permeability TFC membrane. Liu et al. [22] introduced the synthesized hydrophobic nanofillers into the active layer of poly (piperazine amide), reduced the crosslinking degree of PA layer by inhibiting the diffusion rate of piperazine, and prepared TFN membrane with higher water flux. Xu et al. [23] used glycerin as an aqueous phase additive to limit the diffusion of amine monomers to synthesize polyamide nanofiltration membranes with a thickness of 32.3–5.6 nm. The water flux was increased by 51% and the rejection of Na_2SO_4 was maintained at 99.4%. Zhang et al. [24] used hyperbranched polyester (HPE) to interfere with interfacial polymerization. The steric hindrance effect of HPE and the hydrogen bond between HPE and PIP reduced the diffusion rate of PIP. The water flux of the prepared nanofiltration membrane reached $50.62 \text{ L}\cdot\text{m}^{-2}\cdot\text{h}^{-1}\cdot\text{bar}^{-1}$. Wu et al. [25] used phytate (PADS) as an aqueous phase additive to effectively regulate the IP process by using the electrostatic interaction between PADS and amine monomers. The prepared PA-PADS-3 membrane has a water flux of $21.24 \text{ L}\cdot\text{m}^{-2}\cdot\text{h}^{-1}\cdot\text{bar}^{-1}$. However, the restricting behavior of aqueous phase additives on PIP monomers is relatively single at present, only considering the interaction between monomers, or only changing the environmental parameters such as aqueous phase viscosity.

Polyacrylic acid (PAA) is a common water-soluble polymer in industry [26], with rich carboxyl groups, high charge

density, strong mechanical structure through cross-linking, etc. The membrane prepared by PAA is widely used in ultrafiltration, nanofiltration, pervaporation and other separation processes [27–32]. In this study, PAA was used as an aqueous phase additive. There are electrostatic interaction [33] and hydrogen bond interaction [34] between PAA and PIP, and the introduction of PAA increases the viscosity of aqueous solution. The combination of the two factors reduces the diffusion rate of PIP to the organic phase, making it possible to thin the separation layer (Fig. 1). The optimized PAA_0.15@PA membrane has the surface characteristics of rougher, more hydrophilic and more negative. While maintaining a higher flux, the membrane has excellent salt rejection performance. The prepared membrane has a narrower pore-size distribution, high rejection rate for small molecule (180–400 Da) organics, and good separation stability. It provides a new idea for the preparation of high flux nanofiltration membranes by restricted the diffusion of amine monomers.

2. Materials and methods

2.1. Materials

Piperazine (PIP, anhydrous, 99.0%), polyacrylic acid (PAA, M.W. 240000) was purchased from J&K Scientific, trimesoyl chloride (TMC, 98%), polyethylene glycol (PEG, 200, 400, 600, 800, 1000 Da), glucose ($\text{C}_6\text{H}_{12}\text{O}_6$, 99.0%), sucrose ($\text{C}_{12}\text{H}_{22}\text{O}_{11}$, 99.9%) were purchased from Shanghai Aladdin Bio-Chem Technology Co., Ltd., (Shanghai), *n*-hexane (analytically pure), sodium phosphate (Na_3PO_4 , anhydrous, 98.0%), hydrochloric acid (HCl, 36.0%–38.0%), sodium hydroxide (NaOH, 96.0%), sodium sulfate (Na_2SO_4 , 99.0%), magnesium sulfate (MgSO_4 , 98.0%), sodium chloride (NaCl, 99.5%), magnesium sulfate (MgCl_2 , 99.0%) were purchased from Sinopharm Chemical Reagent Co., Ltd., polysulfone (PSF) membrane molecular weight cut-off (MWCO = 35 kDa, pure water flux 570–620 $\text{L}\cdot\text{m}^{-2}\cdot\text{h}^{-1}$) was provided by Huzhou Research Institute of Zhejiang University of Technology, and deionized (DI) water was made by the laboratory.

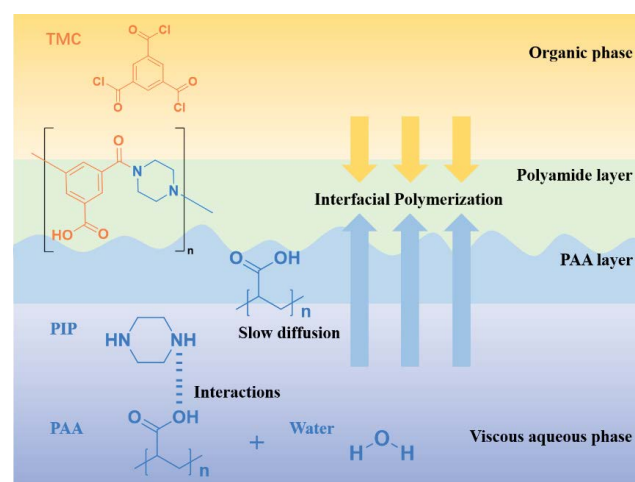


Fig. 1. Schematic diagram of polyacrylic acid restricting piperazine diffusion to prepare nanofiltration membrane.

2.2. Preparation of membranes

The aqueous solution was prepared by evenly dissolving 0.3 wt.% PIP, 2.0 wt.% Na_3PO_4 and a certain amount of PAA (0.00, 0.05, 0.10, 0.15, 0.20, and 0.30 wt.%) in deionized water, and adjusting the pH of the aqueous phase solution to 12 with HCl and NaOH. Among these, Na_3PO_4 acts as a buffer in the system. The aqueous solution was dumped on the PSF base membrane for 2 min to remove residual surface droplets. The organic phase solution was prepared by dissolving 0.1 wt.% TMC in *n*-hexane solvent, dumped onto a PSF base membrane, and drained after contact for 30 s. Heat treatment in an oven at 60°C for 10 min was used as a subsequent optimization process. Finally, the prepared PAA composite membranes of different contents were immersed in deionized water to remove residual monomers and solvents on the membrane surface. The resultant membranes were labeled as pristine PA, PAA_0.05@PA, PAA_0.10@PA, PAA_0.15@PA, PAA_0.20@PA, and PAA_0.30@PA, respectively.

2.3. Characterization of membranes

Field emission scanning electron microscopy (SEM, SU8010 Hitachi, Japan) was used to observe the surface morphology and characterize the cross-section of the film. Transmission electron microscopy (TEM, HT7700 Exalens, Hitachi, Japan) was used to observe the cross-sectional morphology of the film. The membrane surface was characterized by atomic force microscope (AFM, Dimension Icon, Bruker, USA), and the information of membrane surface morphology and roughness was obtained through analysis. X-ray photoelectron spectroscopy (XPS, K-Alpha+, Thermo Scientific, USA) was used to analyze the chemical composition and functional group composition of the membrane surface. The contact angle of water on the membrane surface was measured with a contact angle tester (OCA50AF, Dataphysics, Germany). The solid surface zeta potential tester (SurPASS 3, Anton Paar, Austria) was used to measure the membrane surface potential.

2.4. Determination of relative viscosity

The relative viscosity of aqueous solution was measured by Ubbelohde capillary viscometer. Immerse the capillary viscometer vertically in a 25°C ± 0.1°C thermostatic water bath, and use a stopwatch to time the flow time of solvent and solution in the capillary viscometer, and repeat the measurement for three times. In this experiment, the solvent flow time t_0 is greater than 100 s, so the kinetic energy correction factor can be ignored. The relative viscosity η_r was calculated by Eq. (1):

$$\eta_r = \frac{t}{t_0} \quad (1)$$

where t_0 (s) is the passage time of pure water in the capillary viscosity meter, and t (s) is the passage time of the aqueous phase solution with different PAA additions in the capillary viscosity meter.

2.5. Determination of PIP relative diffusion coefficient

The relative diffusion coefficient of PIP monomer was measured by ultraviolet visible spectrophotometer (UV-Vis, P1, MAPADA, China), as shown in Fig. 2. Add 1.5 mL of aqueous phase solution and pure *n*-hexane into the clean and dry cuvette. Place it in the measuring platform carefully and wait for 30 s to simulate the time of actual interfacial polymerization reaction. The measurement wavelength of ultraviolet light is 232 nm, and the detection target is *n*-hexane solution containing diffused PIP. The relative diffusion coefficient D_r of PIP was calculated by Eq. (2):

$$D_r = \frac{D}{D_0} \quad (2)$$

where D_0 is the absorbance of the target solution without PAA, and D is the absorbance of the target solution with different PAA addition.

2.6. Membrane performance evaluation

The cross-flow filtration system was used to evaluate the separation performance of the membrane. The tested salts are Na_2SO_4 , MgSO_4 , NaCl, MgCl_2 , the concentration of salt solution is 2,000 ppm, the tested small molecule organic substances are glucose, PEG200, sucrose, PEG400, and the concentration of small molecule solution is 500 ppm. The operating pressure is 0.5 MPa, and the feed liquid temperature is kept at 25°C. The effective radius of the membrane sample is 2.5 cm, the effective area is 19.63 cm², and the flow rate on the membrane surface is 0.68 m·s⁻¹. During the test, the membrane is pre-pressed for 30 min at a constant pressure of 0.6 MPa, and then start to receive the filtered permeate. The water flux J (L·m⁻²·h⁻¹) was calculated by Eq. (3):

$$J = \frac{\Delta V}{S \times \Delta t} \quad (3)$$

where ΔV (L) is the volume of the permeable fluid for a certain time, S (m²) is the effective area of the membrane, Δt (h) is the test time. The rejection R (%) was calculated by Eq. (4):

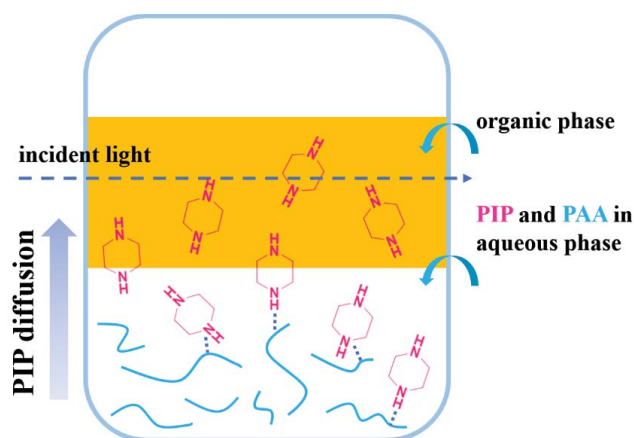


Fig. 2. Schematic diagram of piperazine relative diffusion coefficient measurement.

$$R = \left(1 - \frac{C_p}{C_f} \right) \times 100\% \quad (4)$$

where C_p (ppm) is the concentration of penetrant, and C_f (ppm) is the concentration of feed solution. In a certain concentration range, the concentration of salt solution is proportional to the conductivity. In this experiment, conductivity meter (DDSJ-308A) was used to measure the conductivity of penetrant and feed solution.

The membrane interception MWCO is determined by intercepting PEG, which is the molecular weight corresponding when the PEG interception rate is 90%. The PEG test solution concentration was 1,000 ppm, the operating pressure was 0.5 MPa, and the feed fluid temperature was maintained at 25°C. The concentration of organic matter in the permeate and feed liquid is determined by the total organic carbon analyzer (TOC-LCPH, SHIMADZU, Japan).

The pore-size distribution of the membrane is calculated using the probability density function [35], and it is calculated by Eq. (5):

$$\frac{dR(r_p)}{dr_p} = \frac{1}{r_p \ln \sigma_p \sqrt{2\pi}} \exp \left[-\frac{(\ln \sigma_p - \ln \mu_p)^2}{2(\ln \sigma_p)^2} \right] \quad (5)$$

where r_p (nm) is the aperture, μ_p (nm) is the geometric average radius of PEG when the rejection is 50%, and σ_p (nm) is the ratio of the geometric average radius of PEG when the rejection rate is 84.13% and 50%. The geometric average radius r_s (nm) [36] was calculated by Eq. (6):

$$\log r_s = -1.3363 + 0.395 \log M \quad (6)$$

where M is the molecular weight of the PEG corresponding to a certain rejection rate. The hydrophilicity of the membrane surface can be reflected by the interfacial free energy. According to the water contact angle and AFM characterization results of the membrane surface, the surface energy of the membrane $-\Delta G_{SL}$ ($\text{mJ}\cdot\text{m}^{-2}$) [37] was calculated by Eqs. (7) and (8):

$$-\Delta G_{SL} = \gamma L \left(1 + \frac{\cos \theta}{r} \right) \quad (7)$$

$$r = 1 + \text{SAD} \quad (8)$$

where γL ($\text{mJ}\cdot\text{m}^{-2}$) is the surface tension of liquid ($72.8 \text{ mJ}\cdot\text{m}^{-2}$ for water at 25°C), θ (°) is the water contact angle of the membrane surface, and SAD is the ratio of the difference of surface area and the projected area.

3. Results and discussion

3.1. PIP diffusion study

The introduction of PAA will change the viscosity of aqueous solution. At the same time, the interaction between PAA and PIP (such as electrostatic interaction, hydrogen bonding, etc.) will affect the diffusion rate of PIP, which

will lead to the change of membrane structure [38,39]. Fig. 3 shows the effect of PAA concentration on aqueous viscosity and PIP diffusion. It can be seen that the relative viscosity of aqueous solution increases with the continuous introduction of PAA. It shows that PAA as a polymer can effectively improve the viscosity of aqueous solution environment, and to some extent slow down the diffusion rate of PIP to organic phase. From the simple PIP diffusion experiment, it can also be seen that under the joint influence of the water phase viscosity and the interaction between monomers, the concentration of PIP diffusing to the organic phase in the same time is lower, which can be reflected by the reduction of the relative diffusion coefficient D_r . It shows that the introduction of PAA can restrict the diffusion behavior of aqueous monomer PIP, and the reduction of PIP diffusion rate is helpful to realize the adjustment of the phase structure and separation performance of nanofiltration membrane.

3.2. Element composition on the surface of nanofiltration membrane

Firstly, the surface element composition of the nanofiltration membrane was analyzed by Fourier-transform infrared spectroscopy (FTIR) and XPS. In the FTIR spectra of Fig. 4a, the characteristic peak at $1,630 \text{ cm}^{-1}$ corresponds to C=O vibration, mainly from O=C-N (amide group) generated by the reaction of PIP and TMC, while the characteristic peak at $1,450 \text{ cm}^{-1}$ corresponds to O=C-O (carboxyl group), mainly from the hydrolysis of unreacted acyl chloride groups on TMC and carried by a small amount of PAA itself. Two characteristic peaks confirmed the formation of polyamide. Meanwhile, compared with pristine PA, no new characteristic peak appeared in the PAA@PA membrane. It can be seen from the XPS spectrum of Fig. 4b that three characteristic peaks of C, N and O appear on the surface of pristine PA and PAA@PA membrane. Compared with pristine PA, the PAA@PA membrane has a stronger O1s peak, indicating that the introduction of PAA increases the content of O element on the membrane surface.

In order to better understand the surface composition of the nanofiltration membrane, the O1s peak of the pristine

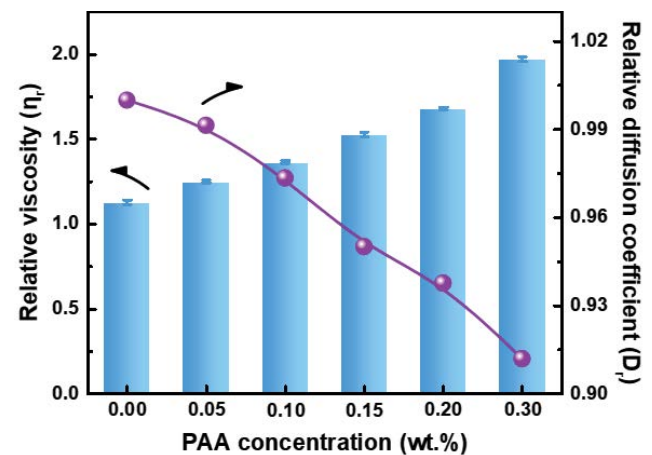


Fig. 3. Effect of polyacrylic acid concentration on aqueous phase viscosity and piperazine diffusion.

PA and PAA@PA membrane were separated. As shown in Fig. 5, the O1s narrow scanning spectrum of 528–536 eV can be divided into two characteristic peaks, namely, O=C–N (amide group) of 532.0 eV and O=C–O (carboxyl group) of 533.5 eV [37]. With the continuous addition of PAA, the

proportion of amide group decreased (62.52% vs. 59.34%) and the proportion of carboxyl group increased (37.48% vs. 40.66%). This is because after the introduction of PAA, the number of PIP molecules diffused to the organic phase to react with TMC in the interfacial polymerization process

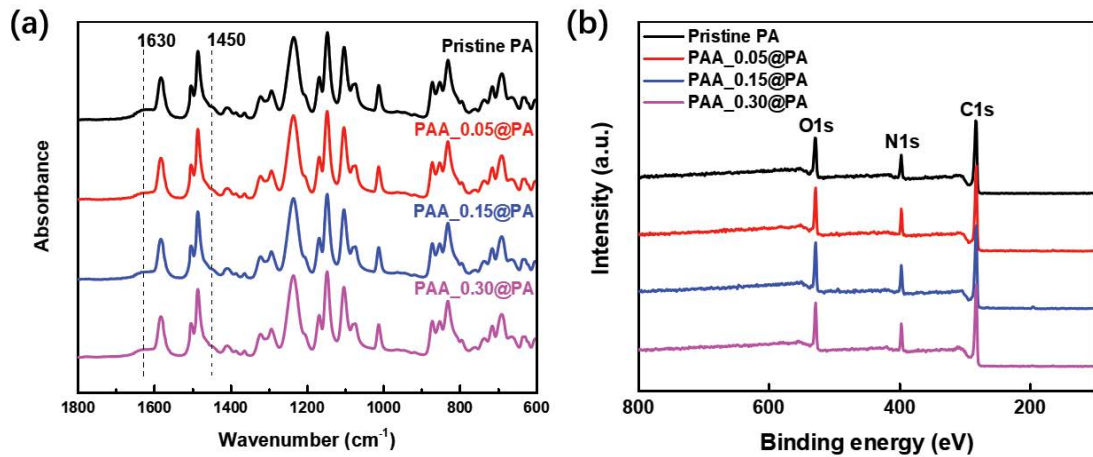


Fig. 4. (a) Fourier-transform infrared spectra and (b) X-ray photoelectron spectrum of pristine PA and PAA@PA membrane.

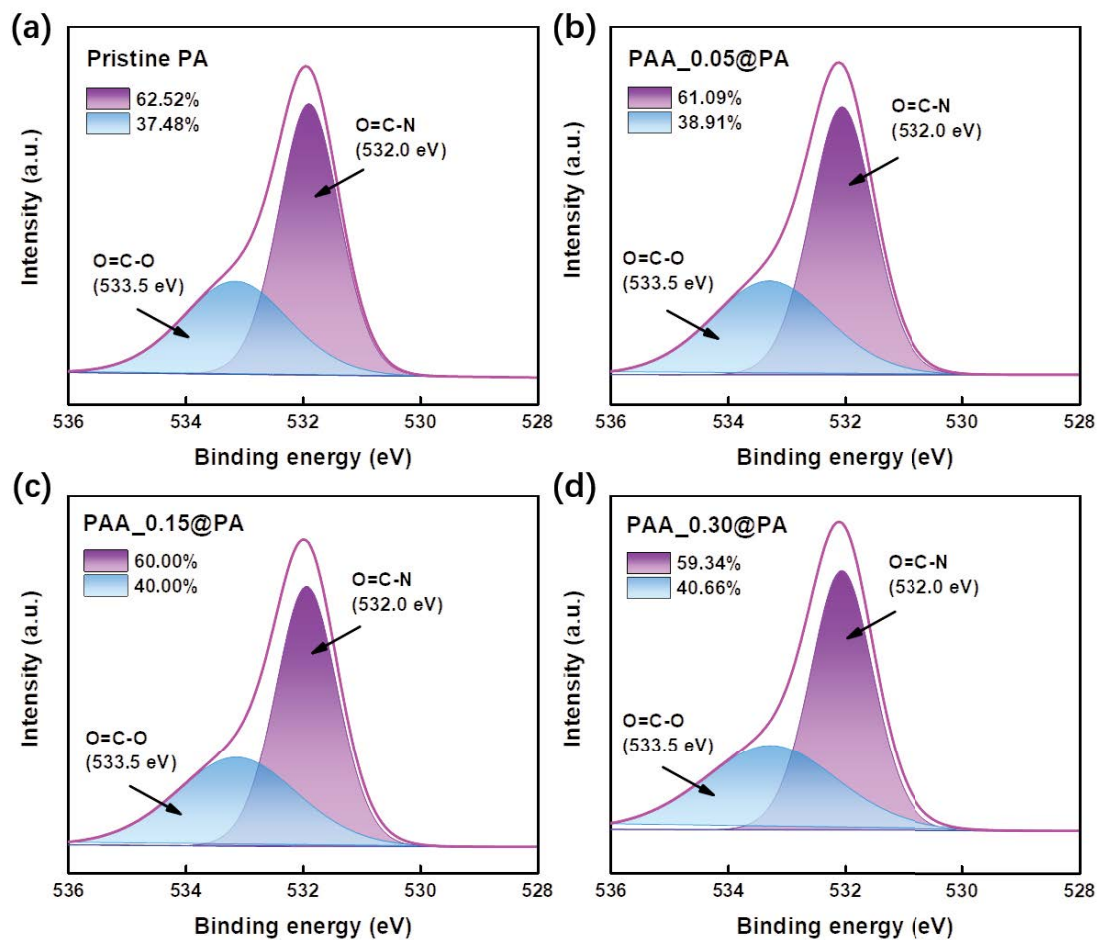


Fig. 5. O1s peak spectrum of membrane surface: (a) pristine PA, (b) PAA_0.05@PA, (c) PAA_0.15@PA and (d) PAA_0.30@PA.

decreases, and the actual reaction area is correspondingly reduced and uneven, and the membrane surface is prone to form defect exposed PAA molecules. Of course, insufficient supply of PIP molecules will also lead to excess TMC in the organic phase. Unreacted acyl chloride groups will hydrolyze to carboxyl groups, and the increase in the proportion of carboxyl groups will enhance the membrane surface electronegativity.

3.3. Morphology of nanofiltration membrane

Fig. 6 shows the SEM images of the pristine PA and PAA@PA membrane surfaces. Fig. 6a presents the typical globular nodule morphology on the surface of the polyperazine amide nanofiltration membrane [40]. With the introduction of PAA, the globular nodules on the membrane surface gradually evolved into a long-chain “pearl string” appearance, and began to become dense with the increase

of addition, as shown in Fig. 6b–f. At a greater magnification, as shown in Fig. 6b–d, the introduction of PAA causes the spherical structure growth of a part of the membrane surface to become circular and stacked with each other. This change in microscopic morphology affects the membrane surface morphology and changes macro, resulting in increased roughness and hydrophilicity, and then improving the water flux of the membrane. When the PAA addition amount exceeds 0.2 wt.%, the morphology of the membrane surface changed significantly, and the appearance of the long chain “pearl string” gradually disappeared, which may be due to the excessive growth of the spheroid structure at the micro scale, the collapse turned into a flat cake structure, the membrane surface began to become smooth, the roughness decreased, which is one of the reasons why the membrane water flux began to decrease.

The roughness and the effective permeability area of the nanofiltration membrane have a great influence on the

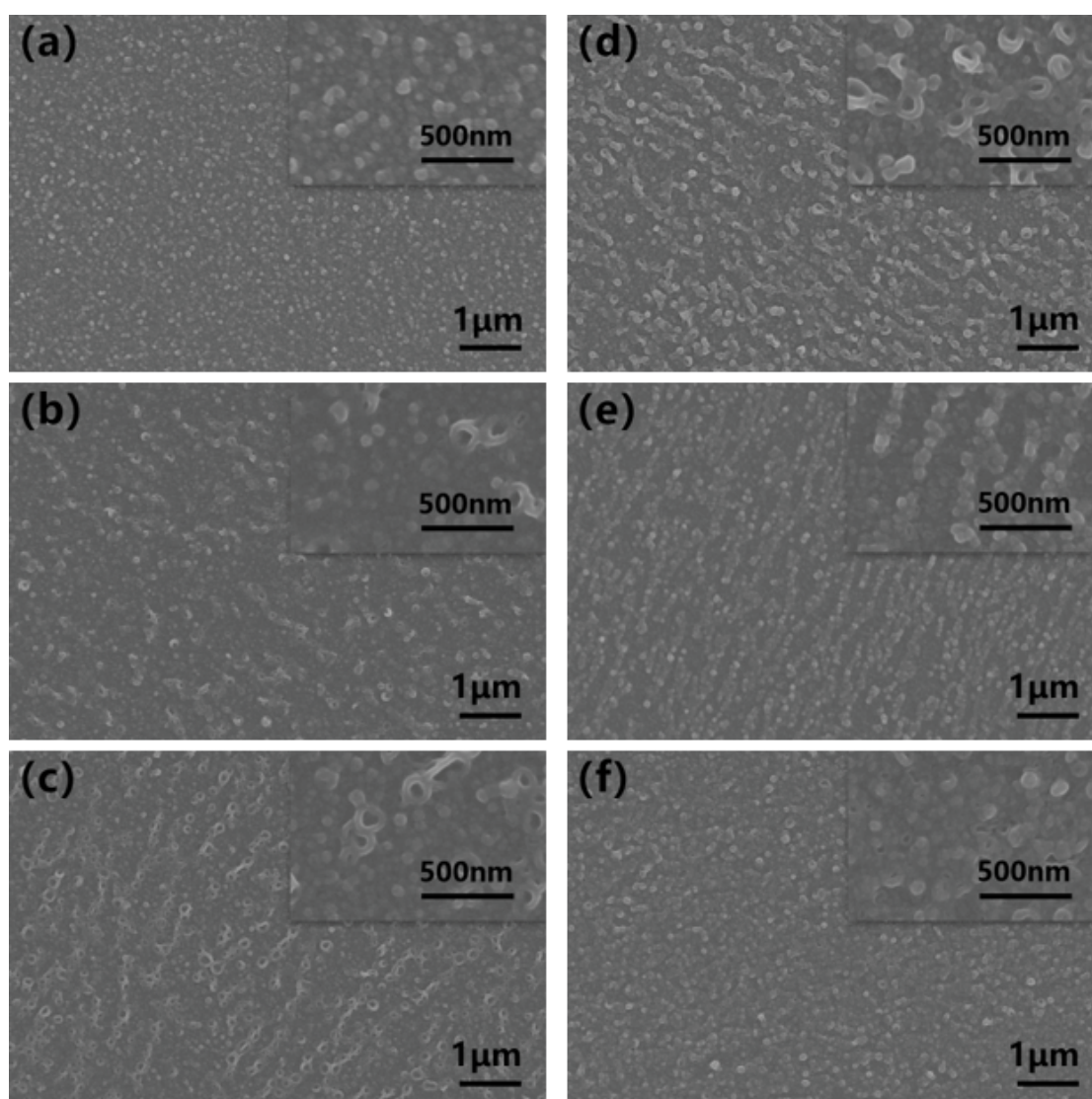


Fig. 6. Scanning electron microscopy images of membrane surface: (a) pristine PA, (b) PAA_0.05@PA, (c) PAA_0.10@PA, (d) PAA_0.15@PA, (e) PAA_0.20@PA and (f) PAA_0.30@PA.

separation performance of the membrane. According to the 3D AFM diagram of the membrane surface (Fig. 7), the roughness of the PAA@PA membrane surface increases compared to the pristine PA. With the addition of PAA, the roughness of the membrane surface first increases, and then decreases. When the PAA addition amount is 0.15 wt.%, the roughness of the membrane surface reached the maximum, with $R_a = 18.65 \pm 0.45$ nm. The change in membrane surface roughness is consistent with the SEM morphology characteristics. At the same time, the cross-section of pristine PA and PAA_0.15@PA membrane were observed by TEM (Fig. 8), it can be observed that there is a layer of fold structure on the PSF base membrane, which is the PA separation layer. The fold structure on the surface of the PA layer grows towards the organic phase side. The introduction of PAA leads to the increase of the fold scale, which corresponds to the change of the membrane surface roughness in Fig. 7a and d.

Next, in order to understand the influence of the introduction of PAA on the membrane separation layer thickness, the membrane cross-section was characterized by SEM. As

shown in Fig. 9a–d, the separation layer thickness of the membrane gradually decreases with the addition of PAA, and the thickness decreased from 96.64 to 62.84 nm at the addition amount of 0.15 wt.%. When the addition of PAA continues, the thickness of the separation layer begins to increase again, as shown in Fig. 9d–f. As a polymer, PAA aqueous solution also shows strong viscosity. At the same time, the molecular weight of PAA selected in this work is 240,000, which is far greater than PIP. When the aqueous solution containing PIP and PAA is poured onto the base membrane for 2 min, PAA will sink to the bottom. One end is adhered to the base membrane, and the other end restricts the diffusion of PIP to the organic phase. Therefore, it can be abstractly considered that the separation layer is a composite layer of PA and PAA. The increase of the viscosity of water phase reduces the thickness of PA layer, while the introduction of PAA increases the thickness of PAA layer. The two show a game relationship of “one decreases and the other increases”, which may be the reason why the overall thickness of the separation layer increases first and then decreases.

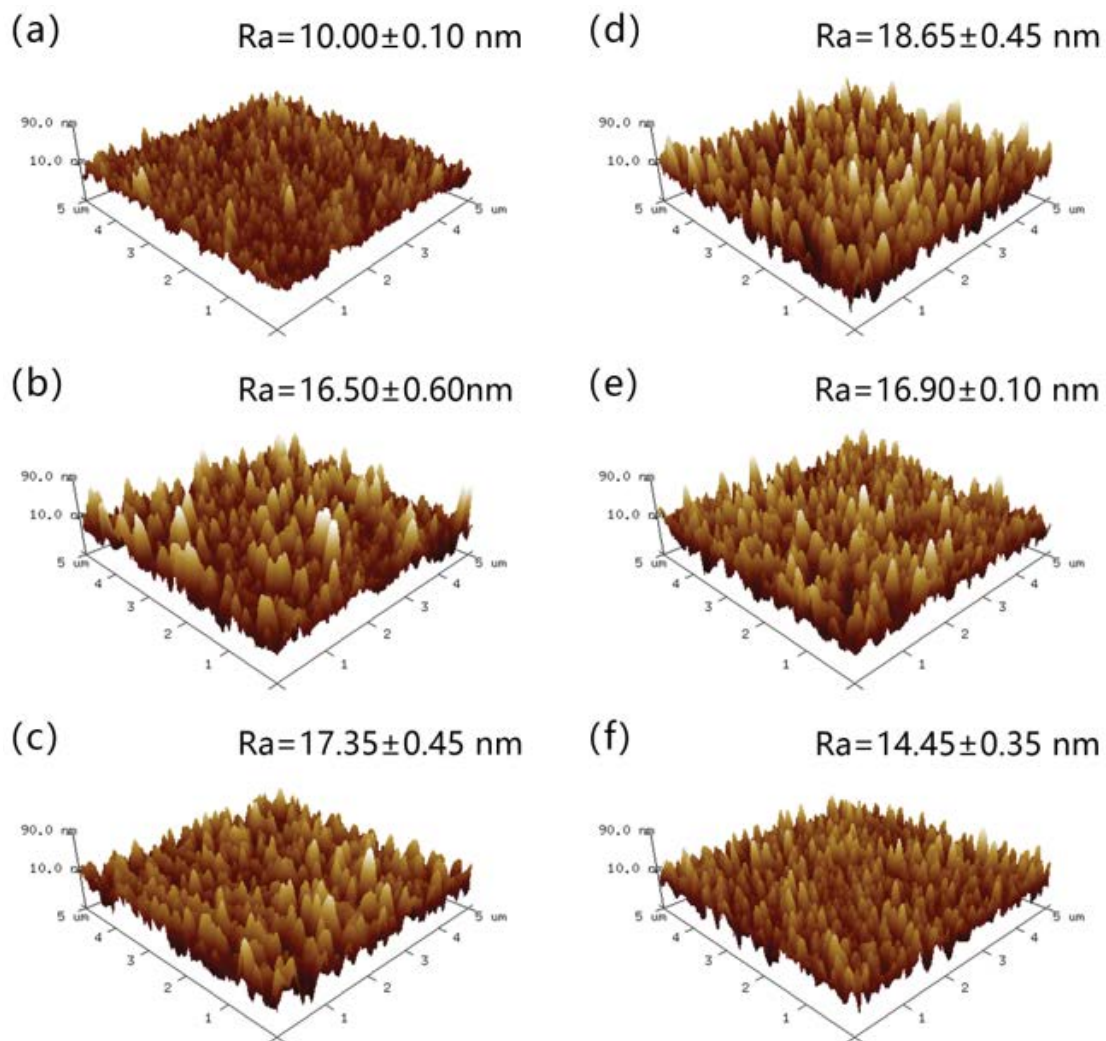


Fig. 7. Atomic force microscope images of membrane surface: (a) pristine PA, (b) PAA_0.05@PA, (c) PAA_0.10@PA, (d) PAA_0.15@PA, (e) PAA_0.20@PA and (f) PAA_0.30@PA. Scan size: $5 \mu\text{m}^2 \times 5 \mu\text{m}^2$. R_a : average roughness.

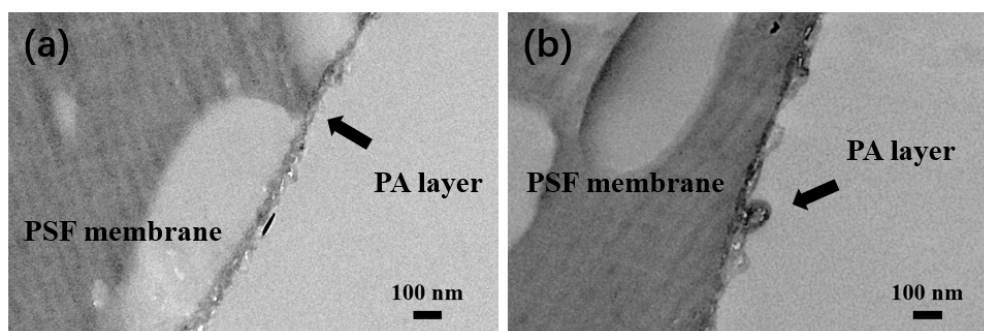


Fig. 8. Transmission electron microscopy images of membrane cross-section: (a) pristine PA and (b) PAA_0.15@PA.

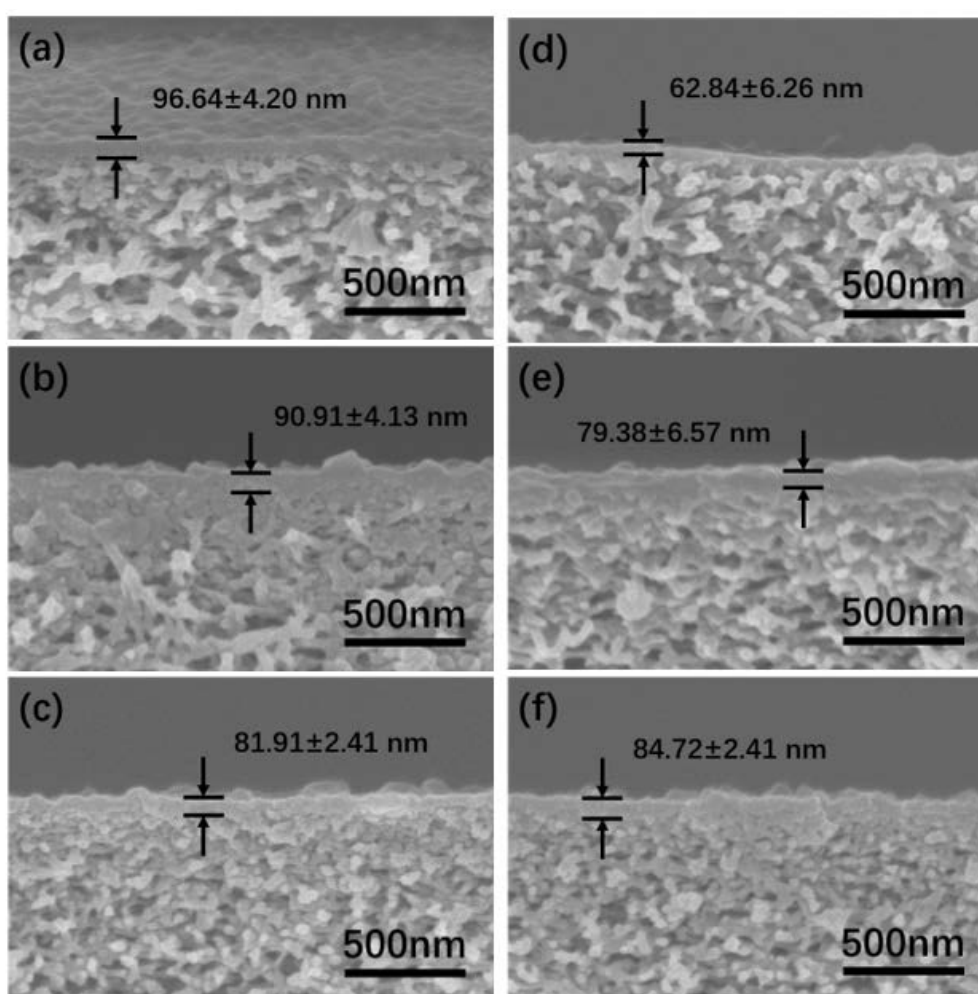


Fig. 9. Scanning electron microscopy images of membrane cross-section: (a) pristine PA, (b) PAA_0.05@PA, (c) PAA_0.10@PA, (d) PAA_0.15@PA, (e) PAA_0.20@PA and (f) PAA_0.30@PA.

3.4. Pore-size distribution, hydrophilicity and zeta potential of nanofiltration membrane

Fig. 10a shows the intercepted molecular weights of pristine PA and PAA@PA membrane, and it can be seen that the MWCO values of pristine PA, PAA_(0.05,0.10)@PA membrane are about 390 Da, while the MWCO values of

PAA_(0.15,0.20,0.30)@PA membrane are about 340 Da. As shown in Fig. 10b, the effective aperture of the membrane decreased (0.29 vs. 0.32 nm) and the pore-size distribution became narrower. The amine group of PIP is positively charged, while the carboxyl group of PAA is negatively charged, so there is electrostatic interaction between them. At the same time, there is a hydrogen bond between H and

the amino group of PIP and O on the carboxyl group of PAA. The introduction of PAA takes advantage of the interaction with PIP on the one hand, and also changes the viscosity of the water phase on the other hand. Under the joint action of the two factors, the diffusion rate of PIP to the organic phase is effectively restricted, and the polymerization reaction at the interface is more complete. Finally, a narrower pore-size distribution and a firm separation layer structure are formed.

The effect of different PAA content on the hydrophilicity of the membrane was investigated by measuring the water contact angle of the membrane surface. As shown in Fig. 11a, the water contact angle decreased from 46.5° to 37.1° when PAA was gradually added to 0.15 wt.%, and then rose to 44.35° with further addition of PAA. Considering that the water contact angle is mainly determined by both the hydrophilicity and the roughness of the membrane surface together, the surface energy $-\Delta G_{SL}$ of membrane is calculated to further reflect the wetting properties of the membrane surface. As you can see, the value of $-\Delta G_{SL}$ was increased from 118.99 to 123.02 $\text{mJ}\cdot\text{m}^{-2}$ and then reduced to 118.58 $\text{mJ}\cdot\text{m}^{-2}$. It shows that the membrane surface hydrophilic character is first enhanced and then weakened. Based on the XPS and AFM results, it can be considered that the introduction

of PAA leads to more hydrophilic carboxyl group residues on the membrane surface, while the increased roughness makes the membrane surface wetting performance become better, when the added amount was more than 0.15 wt.%, the membrane surface tends to be smooth and the reduction of roughness leads to the gradual weakening of hydrophilicity on the membrane surface. As can be seen from Fig. 11b, PAA_0.15@PA has a lower zeta potential, indicating that the introduction of PAA enhances the electronegativity of the membrane surface.

3.5. Performance evaluation of nanofiltration membrane

The separation performance of nanofiltration membranes with different PAA concentrations was analyzed. With the addition of PAA, the pure water flux of the membrane showed a trend of increase first and then decrease, when the added amount was 0.15 wt.%, the pure water flux reached a maximum of $80.18 \text{ L}\cdot\text{m}^{-2}\cdot\text{h}^{-1}$, nearly 25% higher than pristine PA membrane. As shown in Fig. 12b, when the concentration of PAA increases to 0.15 wt.%, the water flux was increased from 59.88 to $69.38 \text{ L}\cdot\text{m}^{-2}\cdot\text{h}^{-1}$. At the same time, the rejection of Na_2SO_4 remained between 96.2%–97.4%.

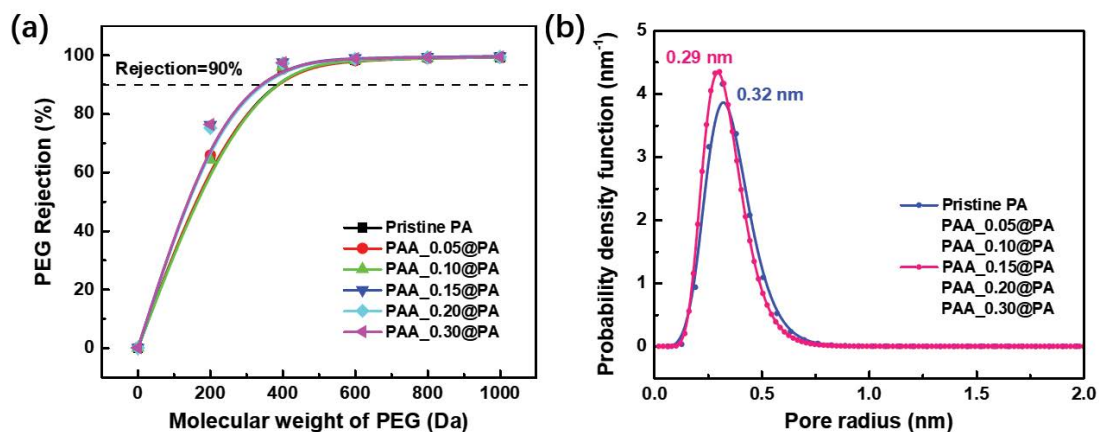


Fig. 10. (a) Molecular weight cut-off and (b) pore-size distribution of pristine PA and PAA@PA membrane.

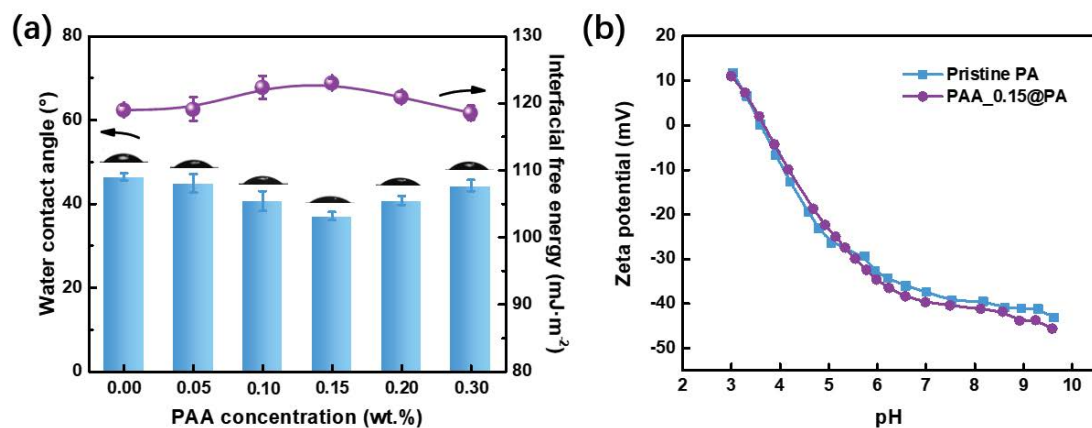


Fig. 11. (a) Effect of polyacrylic acid concentration on water contact angle and interfacial free energy of membranes and (b) zeta potential values of pristine PA and PAA_0.15@PA membrane.

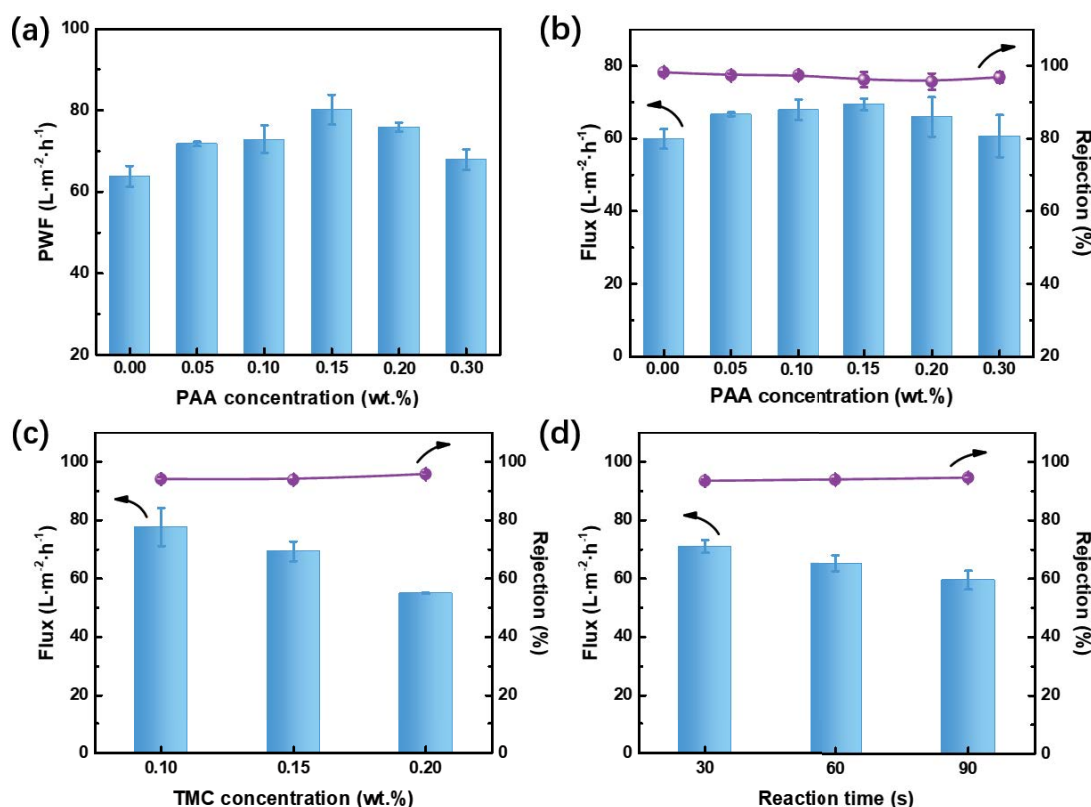


Fig. 12. (a) Effect of polyacrylic acid concentration on pure water flux of membranes; effect of (b) polyacrylic acid concentration, (c) trimesoyl chloride concentration and (d) reaction time on separation performance of membranes.

Because the addition of PAA generated separate layers with rougher surfaces and less thickness. When continuing to add the PAA to 0.3 wt.%, the water flux of the membrane began to decrease to $60.68 L \cdot m^{-2} \cdot h^{-1}$. The rejection was maintained at 97.0%, as caused by the addition of PAA increasing the overall thickness of the separation layer while decreasing the surface roughness. Then, the influence of different TMC concentration and reaction time on the separation performance of nanofiltration membrane was analyzed. From Fig. 12c and d, the increase of the TMC concentration and the prolonged reaction time both led to a significant decrease in the water flux of the membrane, while the rejection of Na_2SO_4 is increased slightly, because the larger TMC concentration and the longer reaction time will make the interface polymerization reaction to some extent more complete, generating a denser separation layer. Therefore, considering the effect of all factors on the nanofiltration membrane separation performance comprehensively, it is determined the PAA concentration of 0.15 wt.%, the TMC concentration was 0.1 wt.%, the reaction time of 30s was the most appropriate.

Furthermore, the separation performance of pristine PA and PAA_0.15@PA membrane for inorganic salts and small molecule organics was compared. As can be seen from Fig. 13a and b, for the four inorganic salts, the PAA_0.15@PA shows a higher water flux than the pristine PA membrane, with a slight decrease in the interception rate, possibly due to the accelerated passage rate of the ions in the face of a thinner separation layer. Meanwhile, the interception order of

the four salts was $Na_2SO_4 > MgSO_4 > NaCl > MgCl_2$. It was a typical charge-negative nanofiltration film, which coincides with the zeta potential results on the membrane surface. As can be seen from Fig. 13c and d, the PAA_0.15@PA membrane exhibited higher water fluxes while maintaining high rejection for the four small molecules (180–400 Da), mainly due to its thinner and rougher separation layer and narrower pore-size distribution. All the above show that PAA is a very ideal aqueous phase additive.

The long-term stability of the nanofiltration membrane is also a major aspect of the performance evaluation. As shown in Fig. 14, the long-term stability of the PAA_0.15@PA membrane for the separation performance of Na_2SO_4 solution (2,000 ppm) and sucrose solution (500 ppm) was tested. For the Na_2SO_4 solution, the water flux of the membrane ($\sim 70 L \cdot m^{-2} \cdot h^{-1}$) and the interception rate ($\sim 96.0\%$) both remained stable. For sucrose solutions, the membrane exhibited relatively constant water flux ($\sim 60 L \cdot m^{-2} \cdot h^{-1}$) and high interception rate ($\sim 99.0\%$). The stability test of the two systems of salt and small molecule organic matter indicated that the PAA_0.15@PA membrane has good structure and stable separation properties.

Finally, the performance of PAA_0.15@PA membrane was compared with commercial membrane (such as NF40, NF90, etc.) and nanofiltration membrane prepared by restricting PIP diffusion reported in the literature, as shown in Table 1. It can be seen that the water flux of these nanofiltration membranes ranges from 2.15 to $14.05 L \cdot m^{-2} \cdot h^{-1} \cdot bar^{-1}$,

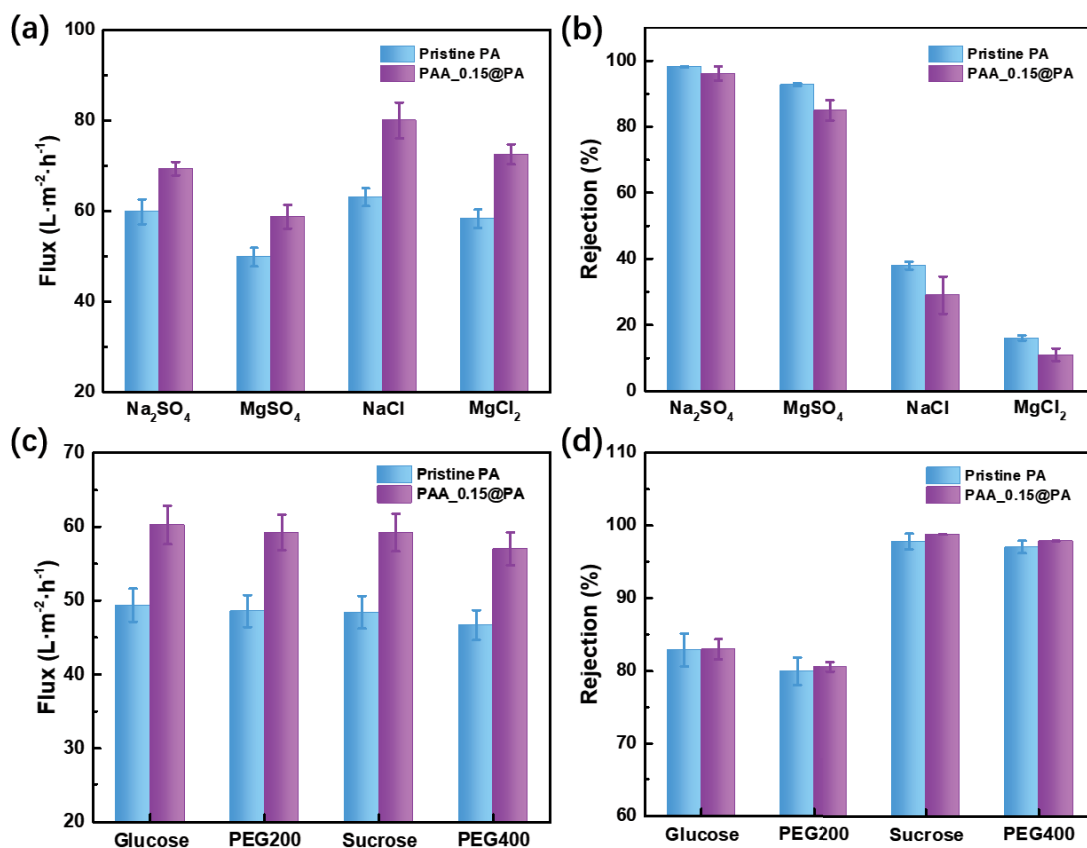


Fig. 13. Separation performance of pristine PA and PAA_0.15@PA membrane for inorganic salts: (a) water flux, (b) rejection; separation performance for small molecule organics: (c) water flux, and (d) rejection.

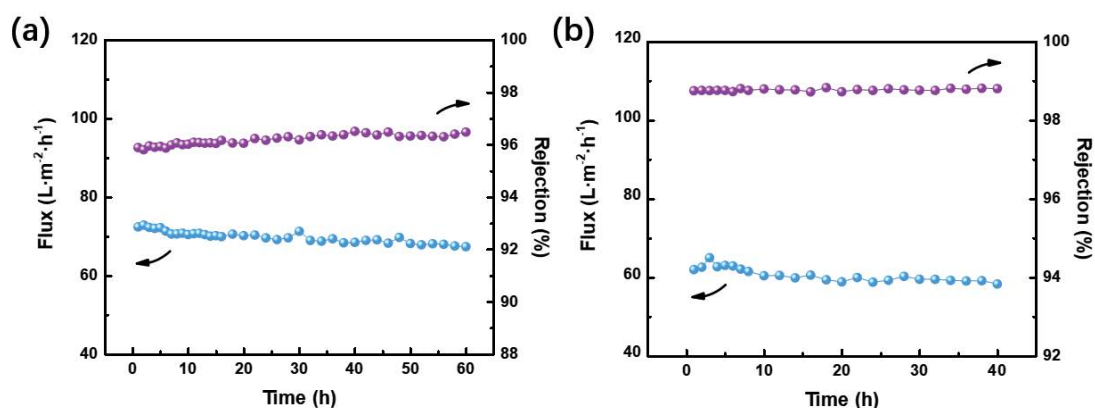


Fig. 14. Long-time operation stability of PAA_0.15@PA membrane: (a) Na_2SO_4 and (b) sucrose.

and the rejection of Na_2SO_4 is 93.5% to 99.6%. The water flux and selectivity of PAA_0.15@PA membrane prepared in this work are higher than that of most advanced nanofiltration membranes at present. The high flux of PAA_0.15@PA membrane is mainly attributed to the effective restriction of PAA on the diffusion of PIP in the process of interfacial polymerization. Its simple preparation process provides a promising strategy for obtaining high flux nanofiltration membrane.

4. Conclusions

In order to effectively restrict the diffusion of piperazine (PIP) monomer to organic phase to prepare high flux nanofiltration membranes, relevant experiments were carried out based on the idea of aqueous phase additives. In this study, polyacrylic acid (PAA) was selected as an aqueous additive to prepare nanofiltration membranes through interfacial polymerization, and a series of characterization analysis

Table 1
Performance comparison between PAA_0.15@PA membrane and other nanofiltration membranes

Membrane	Operating pressure (bar)	Na ₂ SO ₄ concentration (×10 ³ ppm)	Flux (L·m ⁻² ·h ⁻¹ ·bar ⁻¹)	Rejection (%)	References
NF40	5	4.3	2.15	95.0	[41]
NF90	2	1.0	6.86	99.2	[25]
NF270	2	1.0	12.55	99.1	[25]
UTC-60	5	4.3	8.00	98.0	[41]
EB-PIP (4:1)	4	1.0	14.05	98.8	[42]
PA/PD-PES	2	1.0	11.40	93.5	[43]
PA-Tg-0.06	6	2.0	12.00	99.0	[44]
TFC _{0.6}	5	2.0	7.06	98.5	[45]
TFN3	8	1.0	8.97	95.8	[22]
TFC-BDSA	10	2.0	12.20	99.6	[46]
PAA_0.15@PA	5	2.0	13.88	96.2	This work

and performance evaluation were carried out. The specific conclusions are as follows:

- PIP diffusion research experiments show that the introduction of PAA will increase the viscosity of aqueous solution, coordinate the interaction with PIP, slow down the diffusion rate of PIP to the organic phase, and obtain a thinner separation layer.
- The surface element composition, morphology, pore-size distribution, hydrophilicity and zeta potential of the nanofiltration membrane were characterized and analyzed. The results showed that PAA was successfully introduced into the separation layer, resulting in a rougher, more hydrophilic and more negative membrane surface, and a narrower pore-size distribution.
- Performance evaluation of PAA_0.15@PA membrane prepared under optimal conditions: the pure water flux of the membrane was up to 80.18 L·m⁻²·h⁻¹ at 25°C and 0.5 MPa, which was nearly 25% higher than that of the pristine PA membrane. The rejection of Na₂SO₄ solution (2,000 ppm) was 96.2%, and a stable flux of ~70 L·m⁻²·h⁻¹ was maintained. For four small-molecule organic compounds (glucose, PEG200, sucrose, PEG400, 180–400 Da), higher water flux were demonstrated while maintaining high rejection. Moreover, long-term stability tests were conducted for both salt and small molecule organic two systems, which showed that the membrane has good structure and stable separation properties.

Author contributions

Ziliang Fan: Investigation, Visualization, Formal analysis, Investigation, Writing-original draft.

Fangwei Chen: Validation.

Wentao Yan: Review and editing.

Yong Zhou: Conceptualization, Methodology, Writing-Review & Editing, Funding acquisition.

Congjie Gao: Supervision, Resources.

Acknowledgments

This work has been strongly supported by the National Key R&D Program of China (Grant No. 2021YFB3801103). Thanks for the scientific research support provided by Center for Membrane and Water Science & Technology.

Conflicts of interest

The authors declare that they have no known competing financial interests or personal relationships that could have appeared to influence the work reported in this paper.

References

- [1] A.W. Mohammad, Y.H. Teow, W.L. Ang, Y.T. Chung, D.L. Oatley-Radcliffe, N. Hilal, Nanofiltration membranes review: recent advances and future prospects, *Desalination*, 356 (2015) 226–254.
- [2] Z.Z. Zhao, S.C. Feng, C.Y. Xiao, J.Q. Luo, W.J. Song, Y.H. Wan, S.H. Li, Exploring ions selectivity of nanofiltration membranes for rare earth wastewater treatment, *Sep. Purif. Technol.*, 289 (2022) 120748, doi: 10.1016/j.seppur.2022.120748.
- [3] Deepti, A. Sinha, P. Biswas, S. Sarkar, U. Bora, M.K. Purkait, Separation of chloride and sulphate ions from nanofiltration rejected wastewater of steel industry, *J. Water Process Eng.*, 33 (2020) 101108, doi: 10.1016/j.jwpe.2019.101108.
- [4] X.Q. Feng, D.L. Peng, J.Y. Zhu, Y. Wang, Y.T. Zhang, Recent advances of loose nanofiltration membranes for dye/salt separation, *Sep. Purif. Technol.*, 285 (2022) 120228, doi: 10.1016/j.seppur.2021.120228.
- [5] W. Zhang, N. Li, X. Zhang, Surface-engineered sulfonation of ion-selective nanofiltration membrane with robust scaling resistance for seawater desalination, *J. Membr. Sci.*, 644 (2022) 120191, doi: 10.1016/j.memsci.2021.120191.
- [6] Y.J. Song, P. Sun, L.L. Henry, B.H. Sun, Mechanisms of structure and performance controlled thin-film composite membrane formation via interfacial polymerization process, *J. Membr. Sci.*, 251 (2005) 67–79.
- [7] Q. Kong, H. Xu, C.W. Liu, G. Yang, M.M. Ding, W. Yang, T. Lin, W. Chen, S. Gray, Z.L. Xie, Fabrication of high performance TFN membrane containing NH₂-SWCNTs via interfacial regulation, *RSC Adv.*, 10 (2020) 25186–25199.
- [8] Z.Y. Ma, X. Zhang, C. Liu, S.N. Dong, J. Yang, G.P. Wu, Z.K. Xu, Polyamide nanofilms synthesized via controlled interfacial polymerization on a “jelly” surface, *Chem. Commun.*, 56 (2020) 7249–7252.
- [9] X.Q. Cheng, Y. Qin, Y.Y. Ye, X.Y. Chen, K. Wang, Y.J. Zhang, A. Figoli, E. Drioli, Finely tailored pore structure of polyamide nanofiltration membranes for highly-efficient application in water treatment, *Chem. Eng. J.*, 417 (2021) 127976, doi: 10.1016/j.cej.2020.127976.
- [10] P.W. Morgan, *Condensation Polymer: By Interfacial and Solution Methods*, Wiley, New York, 1965.
- [11] J.E. Cadotte, US Patent, 4039440, 1977.
- [12] N. Song, Y.C. Sun, X. Xie, D. Wang, F.F. Shao, L.Y. Yu, L.F. Dong, Doping MIL-101(Cr)@GO in polyamide nanocomposite membranes with improved water flux, *Desalination*, 492 (2020) 114601, doi: 10.1016/j.desal.2020.114601.

- [13] B. Wu, N.X. Wang, J.H. Lei, Y. Shen, Q.F. An, Intensification of mass transfer for zwitterionic amine monomers in interfacial polymerization to fabricate monovalent salt/antibiotics separation membrane, *J. Membr. Sci.*, 643 (2022) 120050, doi: 10.1016/j.memsci.2021.120050.
- [14] Y.L. Zhao, G.S. Lai, J.Y. Chong, R. Wang, Dissecting the structure-compactness-performance relationship of thin-film composite polyamide membranes with different structure features, *J. Membr. Sci.*, 654 (2022) 120553, doi: 10.1016/j.memsci.2022.120553.
- [15] Y. Han, S.F. Xu, C. Gao, Ultrathin graphene nanofiltration membrane for water purification, *Adv. Funct. Mater.*, 23 (2013) 3693–3700.
- [16] L.L. Gui, Y.Q. Cui, Y.Z. Zhu, X.Q. An, H.C. Lan, J. Jin, g-C₃N₄ nanofibers network reinforced polyamide nanofiltration membrane for fast desalination, *Sep. Purif. Technol.*, 293 (2022) 121125, doi: 10.1016/j.seppur.2022.121125.
- [17] S. Li, X. Wang, Y.Y. Guo, J.W. Hu, S.D. Lin, Y.Y. Tu, L.H. Chen, Y.H. Ni, L.L. Huang, Recent advances on cellulose-based nanofiltration membranes and their applications in drinking water purification: a review, *J. Cleaner Prod.*, 333 (2022) 130171, doi: 10.1016/j.jclepro.2021.130171.
- [18] Z. Tan, S.F. Chen, X.S. Peng, L. Zhang, C.J. Gao, Polyamide membranes with nanoscale Turing structures for water purification, *Science*, 360 (2018) 518–521.
- [19] K. Chen, P. Li, H.Y. Zhang, H.X. Sun, X.J. Yang, D.H. Yao, X.J. Pang, X.L. Han, Q.J. Niu, Organic solvent nanofiltration membrane with improved permeability by *in-situ* growth of metal-organic frameworks interlayer on the surface of polyimide substrate, *Sep. Purif. Technol.*, 251 (2020) 117387, doi: 10.1016/j.seppur.2020.117387.
- [20] Y.L. Liu, J.Y. Zhu, J.F. Zheng, X.Q. Gao, M.M. Tian, X.M. Wang, Y.F.F. Xie, Y.T. Zhang, A. Volodin, B. van der Bruggen, Porous organic polymer embedded thin-film nanocomposite membranes for enhanced nanofiltration performance, *J. Membr. Sci.*, 602 (2020) 117982, doi: 10.1016/j.memsci.2020.117982.
- [21] S.S. Yuan, G. Zhang, J.Y. Zhu, N. Mamrol, S.L. Liu, Z.H. Mai, P. van Puyvelde, B. van der Bruggen, Hydrogel assisted interfacial polymerization for advanced nanofiltration membranes, *J. Mater. Chem. A*, 8 (2020) 3238–3245.
- [22] Y. Wang, Z.X. Yang, L. Liu, Y.B. Chen, Construction of high performance thin-film nanocomposite nanofiltration membrane by incorporation of hydrophobic MOF-derived nanocages, *Appl. Surf. Sci.*, 570 (2021) 151093, doi: 10.1016/j.apsusc.2021.151093.
- [23] C.Y. Zhu, C. Liu, J. Yang, B.B. Guo, H.N. Li, Z.K. Xu, Polyamide nanofilms with linearly-tunable thickness for high performance nanofiltration, *J. Membr. Sci.*, 627 (2021) 119142, doi: 10.1016/j.memsci.2021.119142.
- [24] J.Y. Tian, B. Song, S.S. Gao, B. van der Bruggen, R.J. Zhang, Omnifarious performance promotion of the TFC NF membrane prepared with hyperbranched polyester intervened interfacial polymerization, *J. Membr. Sci.*, 642 (2022) 119984, doi: 10.1016/j.memsci.2021.119984.
- [25] M.M. Zhang, X.D. You, K. Xiao, Z.Y. Yin, J.Q. Yuan, J.H. Zhao, C. Yang, R.N. Zhang, H. Wu, Z.Y. Jiang, Modulating interfacial polymerization with phytate as aqueous-phase additive for highly-permselective nanofiltration membranes, *J. Membr. Sci.*, 657 (2022) 120673, doi: 10.1016/j.memsci.2022.120673.
- [26] A. Kausar, Poly(acrylic acid) nanocomposites: design of advanced materials, *J. Plast. Film Sheeting*, 37 (2021) 409–428.
- [27] T.H.A. Ngo, D.T. Tran, C.H. Dinh, Surface photochemical graft polymerization of acrylic acid onto polyamide thin-film composite membranes, *J. Appl. Polym. Sci.*, 134 (2017) 44418, doi: 10.1002/app.44418.
- [28] Y.J. Wang, L.F. Liu, J. Xue, J.M. Hou, L. Ding, H.H. Wang, Enhanced water flux through graphitic carbon nitride nanosheets membrane by incorporating polyacrylic acid, *AIChE J.*, 64 (2018) 2181–2188.
- [29] D.M.D. Babiker, L.P. Zhu, H. Yagoub, X.W. Xu, X.J. Zhang, M. Shibraen, S.G. Yang, Hydrogen-bonded methylcellulose/poly(acrylic acid) complex membrane for oil-water separation, *Surf. Coat. Technol.*, 367 (2019) 49–57.
- [30] F.E. Chen, L. Xie, Enhanced fouling-resistance performance of polypropylene hollow fiber membrane fabricated by ultrasonic-assisted graft polymerization of acrylic acid, *Appl. Surf. Sci.*, 502 (2020) 144098, doi: 10.1016/j.apsusc.2019.144098.
- [31] Y.H. Chiao, S.T. Chen, M. Ang, T. Patra, D.A. Castilla-Casadiego, R. Fan, J. Almodovar, W.S. Hung, S.R. Wickramasinghe, High-performance polyacrylic acid-grafted pvdf nanofiltration membrane with good antifouling property for the textile industry, *Polymers*, 12 (2020) 2443, doi: 10.3390/polym12112443.
- [32] W. Han, M.J. Yin, W.H. Zhang, Z.J. Liu, N.X. Wang, K.T. Yong, Q.F. An, Acid-resistance and self-repairing supramolecular nanoparticle membranes via hydrogen-bonding for sustainable molecules separation, *Adv. Sci.*, 8 (2021) 2102594, doi: 10.1002/advs.202102594.
- [33] L.J. Kirwan, P.D. Fawell, W. van Bronswijk, *In-situ* FTIR-ATR examination of poly(acrylic acid) adsorbed onto hematite at low pH, *Langmuir*, 19 (2003) 5802–5807.
- [34] J.C. Ding, H.Q. Wu, P.Y. Wu, Multirole regulations of interfacial polymerization using poly(acrylic acid) for nanofiltration membrane development, *ACS Appl. Mater. Interfaces*, 13 (2021) 53120–53130.
- [35] K.H. Youm, W.S. Kim, Prediction of intrinsic pore properties of ultrafiltration membrane by solute rejection curves: Effects of operating conditions on pore properties, *J. Chem. Eng. Jpn.*, 24 (1991) 1–7.
- [36] W.R. Bowen, A.W. Mohammad, Characterization and prediction of nanofiltration membrane performance – a general assessment, *Chem. Eng. Res. Des.*, 76 (1998) 885–893.
- [37] Y.L. Ji, H.H. Lu, B.X. Gu, R.F. Ye, Y. Zhou, Q.F. An, C.J. Gao, Tailoring the asymmetric structure of polyamide reverse osmosis membrane with self-assembled aromatic nanoparticles for high-efficient removal of organic micropollutants, *Chem. Eng. J.*, 416 (2021) 129080, doi: 10.1016/j.cej.2021.129080.
- [38] A.K. Ghosh, B.H. Jeong, X.F. Huang, E.M.V. Hoek, Impacts of reaction and curing conditions on polyamide composite reverse osmosis membrane properties, *J. Membr. Sci.*, 311 (2008) 34–45.
- [39] Z.Y. Wang, S.M. Liang, Y. Jin, L.R. Zhao, L.J. Hu, Controlling structure and properties of polyamide nanofilms by varying amines diffusivity in organic phase, *J. Membr. Sci.*, 574 (2019) 1–9.
- [40] P. Veerababu, B.B. Vyas, P.S. Singh, P. Ray, Limiting thickness of polyamide-polysulfone thin-film-composite nanofiltration membrane, *Desalination*, 346 (2014) 19–29.
- [41] Z. Yi, F.-d. Wu, Y. Zhou, C.-j. Gao, Novel nanofiltration membranes with tunable permselectivity by polymer mediated phase separation in polyamide selective layer, *Chin. J. Chem. Eng.*, 24 (2016) 1533–1540.
- [42] Z. Liu, Z. Mi, L. Meng, Y. Huang, D. Zhang, J. Wang, K. Zhang, J. Xiao, P. Liu, Z. Rao, H. He, S. Wang, Quaternary ammonium salts modification preparing charged Janus nanofiltration membrane for the simultaneous separation of divalent anions and cations, *J. Membr. Sci.*, 672 (2023) 121440, doi: 10.1016/j.memsci.2023.121440.
- [43] Y.F. Li, Y.L. Su, J.Y. Li, X.T. Zhao, R.N. Zhang, X.C. Fan, J.N. Zhu, Y.Y. Ma, Y. Liu, Z.Y. Jiang, Preparation of thin-film composite nanofiltration membrane with improved structural stability through the mediation of polydopamine, *J. Membr. Sci.*, 476 (2015) 10–19.
- [44] Z. Hao, X. Tian, V. Mankol, Q. Li, J. Wang, Z. Wang, S. Zhao, Polyamide nanofiltration membrane fabricated with ultra-low concentration triaminoguanidine showing efficient desalination performance, *J. Membr. Sci.*, 672 (2023) 121449, doi: 10.1016/j.memsci.2023.121449.
- [45] B. Zhu, R. Shao, N. Li, C. Guo, P. Liu, J. Shi, C. Min, S. Liu, X. Qian, L. Wang, Z. Xu, Narrowing the pore-size distribution of polyamide nanofiltration membranes via dragging piperazines to enhance ion selectivity, *J. Membr. Sci.*, 667 (2023) 121187, doi: 10.1016/j.memsci.2022.121187.
- [46] A.D. Al-Nahari, S.X. Li, B.W. Su, Negatively charged nanofiltration membrane with high performance via the synergistic effect of benzidinedisulfonic acid and trimethylamine during interfacial polymerization, *Sep. Purif. Technol.*, 291 (2022) 120947, doi: 10.1016/j.seppur.2022.120947.